STUDY OF BOUNDARY LAYER FLOW IN ROTATING CURVATURE SYSTEM

(The effects of system rotation and streamline curvature on the secondary instability of the Görtler vortices)

Yutaka Hasegawa
Ecotopia Science Institute, Nagoya University, Furo-cho, Chikusa-ku, Nagoya 464-8603, Japan
hasegawa@mech.nagoya-u.ac.jp

Koji Kikuyama, Michio Nishikawa, and Ryoichi Ihara
Department of Mechanical Engineering, Nagoya University
Furo-cho, Chikusa-ku, Nagoya 464-8603, Japan
kikuyama@mech.nagoya-u.ac.jp, h024103d@mbox.nagoya-u.ac.jp, h034104m@mbox.nagoya-u.ac.jp

ABSTRACT

The behavior of the boundary layer in rotating channels, such as those in impeller passages of turbomachines, is dominantly influenced by the centrifugal and Coriolis forces due to the wall curvature and system rotation, respectively. The resultant force may promote or suppress the instability of the flow in the boundary layer, depending on the direction and magnitude of the component normal to the wall boundary.

The purpose of the present study is to make clear experimentally the effect of the Görtler type instability on a laminar boundary layer and the transition process. The longitudinal changes of velocity and turbulent intensity have been measured near the concave surface. When the Coriolis force whose magnitude exceeds to the centrifugal one acts opposite to the centrifugal force, the generation of the Görtler vortices is suppressed. When the resultant force acts toward the concave surface, the Görtler vortices are generated and develop downstream, resulting in the secondary instability, which leads the boundary layer into a turbulent state.

1. INTRODUCTION

The effects of system rotation or wall curvature on the turbulent boundary layer have been clarified experimentally by some studies (1973)(1979)(1987), and Bradshaw (1969) showed a similarity relationship between the centrifugal force in a curved channel and the Coriolis one in a rotating straight and found that the turbulence in the boundary layer are promoted in the pressure side, and suppressed in the suction side.

On the other hand, in a laminar boundary layer on a concave surface, the Görtler vortices are well known to be generated. Swearingen and Blackwelder (1987), Matsubara and Alfredsson (1998) investigated the boundary layer transition due to the growth or breakdown of the vortices. They found that there are two kinds of the secondary instability, that is, sinuous and varicose modes in the transition process to the turbulent state depending on the magnitude of the force. These phenomena are also closely related to the boundary layer transition near the rotating curvature surface of the impeller passages of centrifugal turbomachines.

The present authors performed a series of experiments for the boundary layer in the rotating curved channel by measuring the time-mean as well as the fluctuating components of velocity and confirmed that the growth and behavior of the Görtler vortices are strongly influenced by the system rotation (2003).

This paper aims at clarifying the effects of system rotation and the wall curvature on the secondary instability of the Görtler vortices and the transition process to the turbulent state.

2. EQUIPMENTS AND METHOD OF EXPERIMENT

Figure 1 shows a schematic outline of the experimental equipment. Two channels of different radii of curvature, R=1,000mm and 2,000mm, are shown to be settled on a rotation table of 3,000mm in diameter. The rotating table supported by thrust bearings can rotate at the rotation speed of 3 to 24rpm both in the clockwise and anti-clockwise directions, so as to change the magnitude of the resultant force. Air was introduced into the channel through a two-dimensional nozzle and exhausted outside through the hollow rotating axis by a blower.

Figure 2 shows the configuration of the measurement section. The high aspect ratio h/d of 8:1 was employed so as to avoid the effects of the top and bottom walls on the flow in the central region of the section. The longitudinal distances of the measuring sections from the leading edge of the plate are listed in Tab. 1 for the channel of R=2,000mm. Velocity measurement was made in the hatched area (y/d=0.01~0.6, z/h=-0.265~0.260) of each section from Sec.1 to Sec. 17, shown in Fig. 2, by traversing a hot-wire probe with 8 sensing wires at the 5 different heights. The Reynolds number, $Re= U_m d/\nu$, based on the free stream velocity in Sec. 1, U_m, and the channel width, d, was taken to be 1.8×10^4 and the dimensionless rotation rate, N, defined by the following equation (1) was taken to be 0, ±0.012, ±0.018, where the sign of N denotes the rotational direction of the channel, that is, the positive value corresponds to the direction where the Coriolis force acts toward the concave wall.

$$N = \Omega d/U_m \qquad (1)$$

It was confirmed that turbulent intensity was less than 0.5% in the uniform inlet flow of the test channel.

In order to evaluate the effects of wall curvature and system rotation, we introduced a new parameter of modified Görtler number, $G' = Re_\theta \sqrt{\theta(1/R + 2N/d)}$ that is the parameter superposing the effect of system rotation on the Görtler number $G = Re_\theta \sqrt{\theta / R}$.

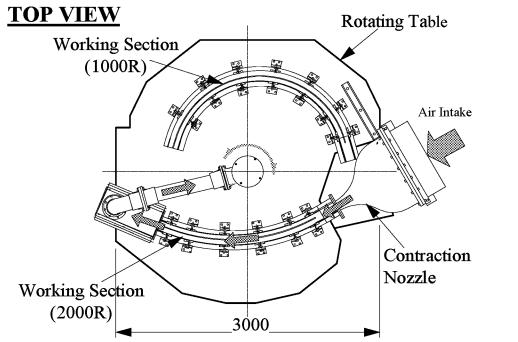

(a) Top view

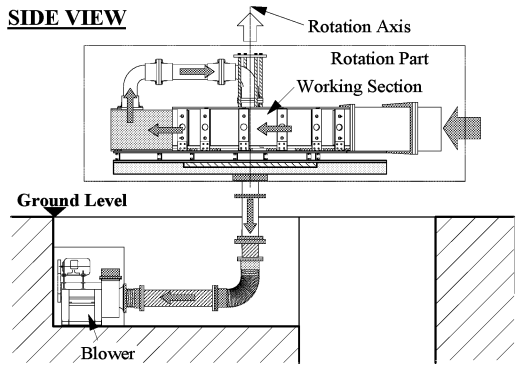

(b) Side wiew

Fig. 1 Schematic outline of experimental setup

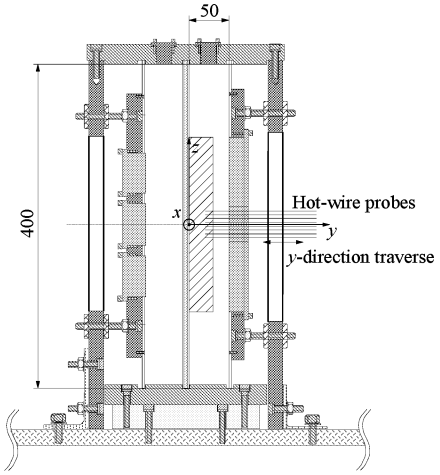

Fig. 2 Configuration and dimensions of cross-seciton

Table 1 Longitudinal distance of measurement sections

Section #	x/d	Section #	x/d	Section #	x/d
Sec.1	2.8	Sec.7	15.6	Sec.13	27.3
Sec.2	5.7	Sec.8	17.5	Sec.14	29.3
Sec.3	7.7	Sec.9	19.5	Sec.15	31.3
Sec.4	9.7	Sec.10	21.5	Sec.16	33.2
Sec.5	11.6	Sec.11	23.4	Sec.17	36.2
Sec.6	13.6	Sec.12	25.4		

3. EXPERIMENTAL RESULTS AND DISCUSSIONS

3.1 Longitudinal change of vortex structure

In the previous work (2003), we confirmed that boundary layer transition to turbulent state was promoted by the increase of the Görtler type instability, when the concave wall was pressure side. In order to obtain the more detail information on the transition process of the boundary layer, simultaneous measurement of the velocity at eight different positions was made.

So as to examine the downstream change in the vortex structure, that is, the merging and dissipation of the Görtler vortices, streaks of low flow velocity obtained in a plane of y/d= 0.08 from the wall for each rotation rate are plotted in Fig. 3 (a) to (e), where the solid lines are drawn along the local minimum velocity points caused by the Görtler vortices.

When the rotation rate N is equal to -0.018 (Fig. 3(a)), the Coriolis force acts away from the wall and its magnitude is larger than that of the centrifugal one. Any noticeable occurrence of low speed region cannot be observed, because the Coriolis force suppresses the generation of the Görtler vortices. The low speed region seen at x/d=25.0 and z/h=0.05 may be due to the secondary flow over the cross section.

For N=-0.012 (Fig. 3(b)), the Coriolis force approximately cancels out the centrifugal one at the free stream and the value of the modified Görtler number G' is about 0.9 which is less than that for the Görtler vortices generation limit, G = 0.3 (Hämmerlin 1955). According to this result, we can found that the low speed region occurs and develops around x/d=10.0, when the body force acting fluid is smaller. In more downstream section, around x/d=30.0, the low speed streak structure becomes unclear at z/h=0.2, 0.1, -0.15, implying the dissipation or breakdown of the Görtler vortices downstream of this section.

For the stationary state N=0 as shown in Fig. 3(c), the generation of low speed region can be found around x/d=10.0. The number of low speed streaks is increased compared with that for N=-0.012, and the decelerated region due to the Görtler vortices is seen to be sustained even in the downstream sections.

For positive rotation rates, N=0.012 and 0.018 (Fig. 3 (d), (e)), the occurrence of the Görtler vortices is seen in more upstream sections and the merging of low speed regions, i.e. the merging of the Görtler vortices, is observed.

As shown in Fig.3, the Görtler vortices, once generated by the centrifugal and Coriolis forces, change their structure due to the secondary instability as they flow downstream.

Figure 4 shows the contour map of time-averaged velocity distribution U/U_m in the area of z/h=0.1~0.24 at the five sections x/d=9.7~17.5 both for N = 0.012 and 0.018. For N=0.012, two neighboring low velocity regions around z/h=0.15 and 0.18 at $x/$

d=9.7 get close to each other in downstream sections and merge around x/d=13.6. For N=0.018, the low velocity regions at z/h=0.17, 0.22, grow in scale without changing their spanwise positions up to x/d=15.6 but they merge into one at x/d=17.5. These merging of vortices are similar to the results of Matsson (1992).

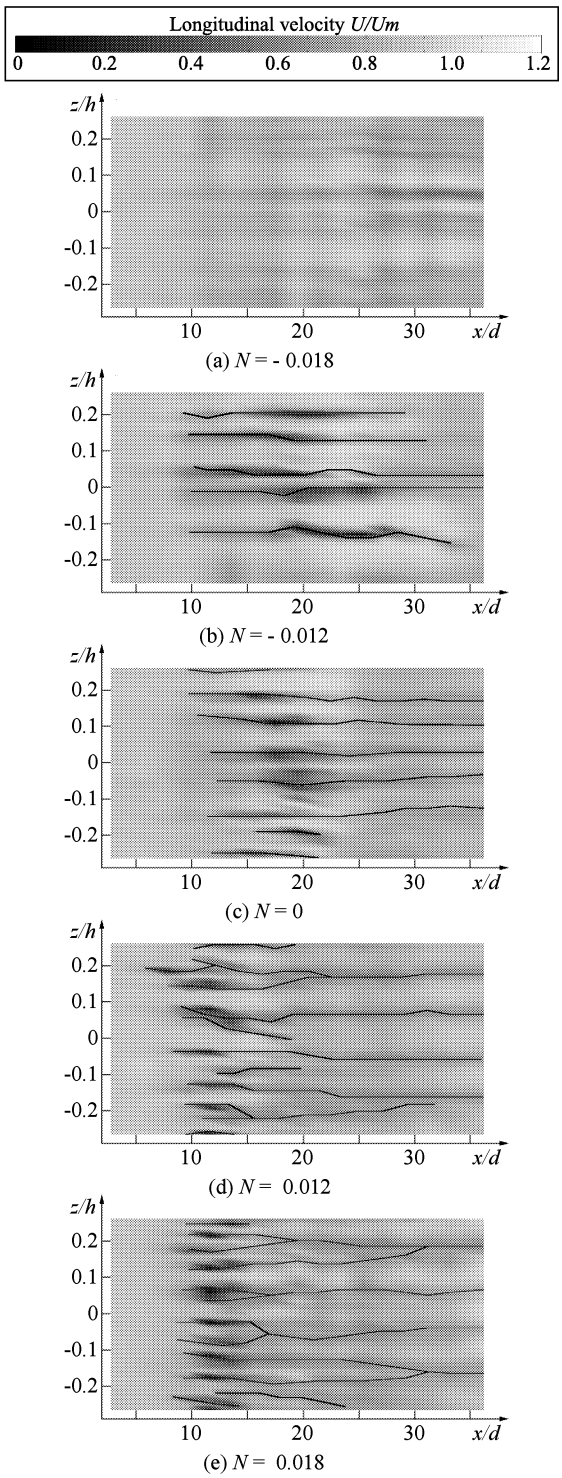

Fig. 3 Low speed streak profile at y/d=0.08 for (a) N = -0.018, (b) N = -0.012, (c) N = 0, (d) N = 0.012, (e) N = 0.018

3.2 The secondary instability of the Görtler flow

In order to examine the development process of the Görtler vortices and their effect on the boundary layer transition to turbulent, we calculate the magnitude of perturbation of the longitudinal velocity, defined by Eq. (2), in each cross-section,

$$E=\left\{\frac{1}{AU_m^2}\iint\left(U(y,z)-\overline{U}(y)\right)^2 dzdy\right\}^{0.5} \quad (2)$$

Figure 5 shows the longitudinal change of E for different rotation rates. Comparing with the generation of the low speed streak in Fig. 3, the magnitude of perturbation, E, for N=-0.012 takes its local maximum value at a section where the configuration of the Görtler vortices is established. Downstream of this section the value of E decreases and reduces to 0.04~0.07 in the downstream sections where the shape factor H of the boundary layer is ascertained to be equal to about 1.4, showing that the boundary layer has shifted into the turbulent state. On the other hand, for the rotation rate of N=-0.018, the value of E gradually increases in streamwise direction as the occurrence of the Görtler vortices is suppressed and the boundary layer still remain laminar.

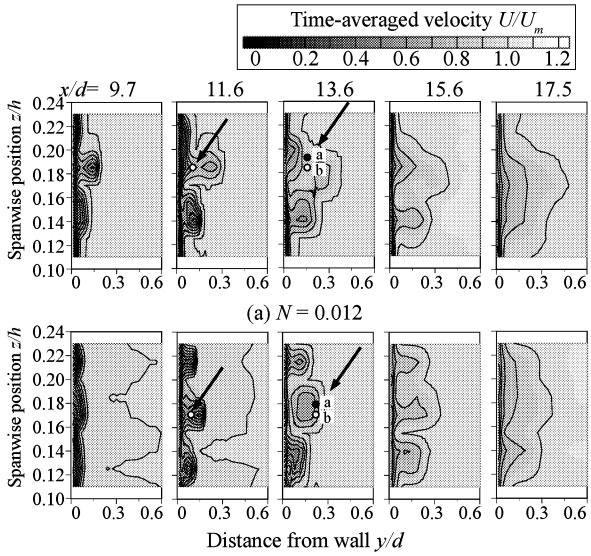

Fig. 4 Time-averaged velocity contour maps

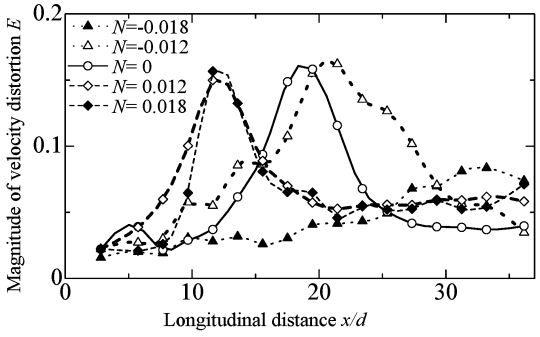

Fig. 5 Longitudinal change of velocity distortion in cross-sectional

By summarizing the detail measurements of velocity profiles and the change in the value of E, we obtained a map of the flow pattern for every rotation rate as shown in Fig. 6. As the rotation rate N increases, the regions of primary instability (generation of the Görtler vortices), secondary instability and transition into turbulent boundary layer, respectively, are found to shift upstream.

3.2.1 The secondary instability for positive rotation rate.

As shown in Fig. 6 the generation of the Görtler vortices has a key effect on the transition to the turbulent state. To examine the transition process, the spectrum density of the fluctuating velocity are measured at the locus of z/h and y/d are 0.185 and 0.15, 0.2, respectively, shown by a white circle in Fig. 4. The spectrum at x/d = 11.6 and 13.6 are shown in Fig. 7. In the section of x/d=11.6 for N=0.012 (Fig. 7(a)) strong peaks appear at 365Hz and at 730Hz, the latter of which is considered as the sub-harmonic frequency of 365Hz. In the downstream section x/d=13.6(Fig. 7(b)), an amplification of 130Hz can also be found.

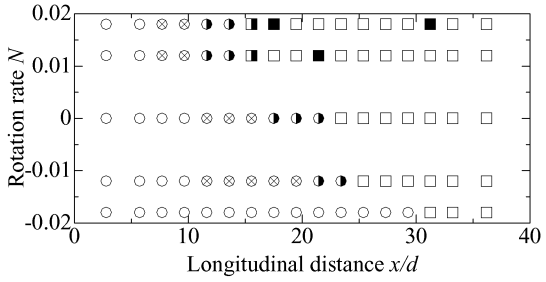

Fig. 6 Distribution of various types of flow pattern (○:laminar state, ⊗:primary instability(Görtler vortices), ◑:secondary instability(varicose & sinuous mode), ◨:secondary instability (merging of vortices pairs), ■:merging of vortices pairs in turbulent state, ▭:turbulent state)

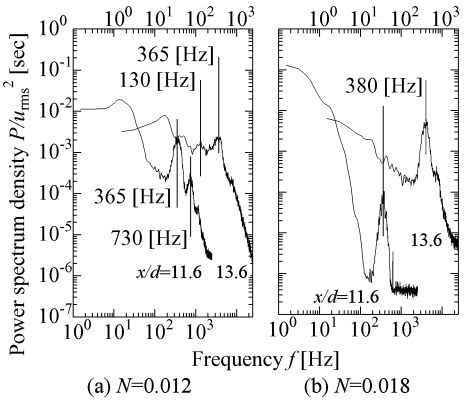

Fig. 7 Power spectrum density at x/d=11.6 and 13.6 (plotted as ○ in Fig. 6)

To examine these fluctuation of the velocity, Fig. 8 shows the comparison of the simultaneous fluctuating velocity at the different two points of a and b denoted in Fig. 6. For N=0.012, (Fig. 8(a)), the fluctuating components filtered at 130 Hz is seen to be in-phase, but that for 365 Hz differs exactly by a half of the cycle. This higher frequency of this fluctuation, 365Hz, is attributable to the sinuous mode of secondary instability, which means that the vortex configuration fluctuates laterally, and the lower one of 130Hz is due to varicose mode of instability (1978) (1994), which means that the horse shoe vortex involves the Görtler vortices pair.

When the rotation is increased to N=0.018, there is a strong amplification at 380Hz in the spectrum density of Fig. 7(b). This instability is considered to be due to the sinuous mode judged from the different phases of the fluctuating velocity.

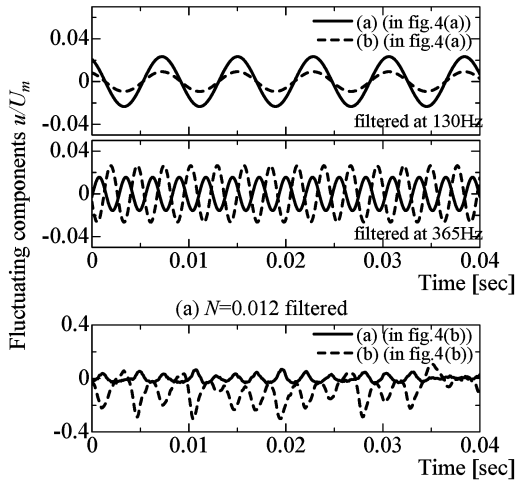

Fig.8 Fluctuating velocity components

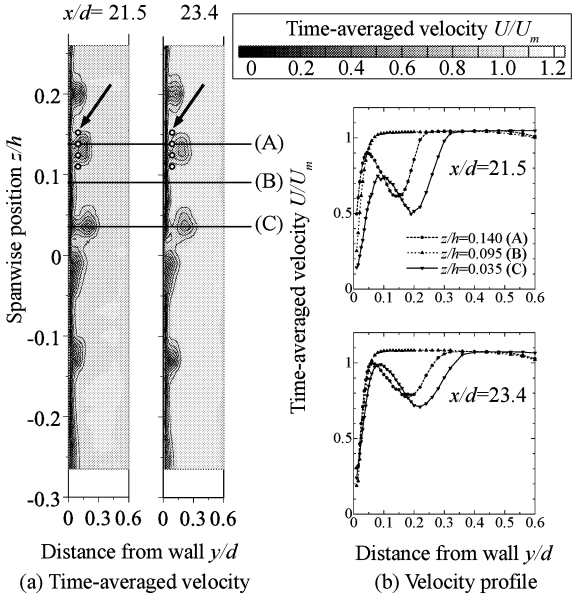

Fig. 9 Time-averaged velocity distribution for N = - 0.012

3.2.2 The secondary instability for negative rotation rate

Figure 9(a)(b) shows the contour map of time-averaged velocity and velocity profiles measured along the lines indicated by (A)~(C) in Fig. 9(a) for N=-0.012. The vortex structure is rather stable in this rotating condition and the generation of the secondary instability may be suppressed, compared with that of positive rotation rates and the velocity profiles on the line of A and C have an inflection point. Figure 10 shows the spectrum density obtained at the positions indicated as circles in Fig. 9(a). The ordinate and abscissa are taken to be non-dimensional spectrum density and frequency, respectively. The peak of the spectrum takes place at the non-dimensional frequency of unity (corresponding to f = 130Hz) (1992). The velocity fluctuations having this frequency are shown in Fig. 11 for different lateral positions of z/h. All of the fluctuating components are exactly in-phase, that is, the varicose mode of secondary instability dominates in this condition.

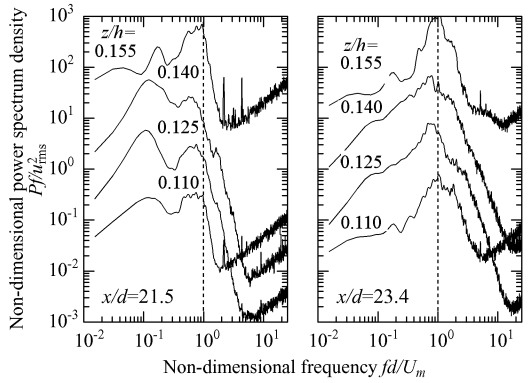

Fig. 10 Power spectrum density at x/d=21.5 and 23.4 for N= - 0.012 (plotted as ○ in Fig. 9(a))

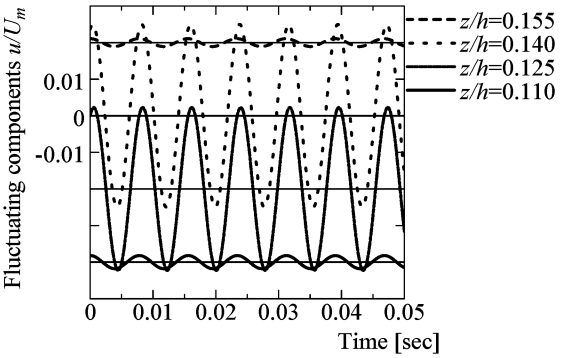

Fig. 11 Fluctuating velocity component filtered at 130Hz at x/d=21.5 for N= -0.012 (plotted as ○ in Fig. 9)

3.3 Interaction between the centrifugal and Coriolis forces

As the type of the secondary instability is found to depend on the rotation rate, that is, the ratio between the centrifugal and Coriolis forces, the transition of the flow pattern are examined for the concave wall of R = 1,000 and 2,000mm. Table 2 shows the list of the ratio employed in the experiments where the centrifugal and Coriolis forces are based on the data in the main flow. The dimensionless value of the resultant force F_r, which is only equal to the sum of two forces, is also listed in Tab. 2. To summarize the primary and secondary instability of the Görtler vortices, Fig. 12 shows the comparison of the downstream change in the flow pattern between R=1,000mm to 2,000mm using the parameter of F_r as the ordinate. Despite of the difference in the radius of the wall curvature, the Görtler vortices are generated almost at the same longitudinal position for F_r=0.52 and 0.5 as well as F_r=1 and 0.98. But the secondary instability and the transition to turbulent state is promoted in more upstream sections in the channel of a larger curvature. From these results, we suggest that the flow pattern in the channel of different curvature may be predicted by using the dimensionless parameter, F_r=1/R+2N/d, which denotes the sum of the effects of centrifugal and Coriolis forces. However, this linear parameter may not be in use for the local effects of the curvature and rotation such as those on the configuration of the Görtler vortices and the secondary superposition.

Table 2 Comparison of the magnitude of centrifugal and Coriolis forces on free stream among different wall curvatures (Force ratio to the centrifugal force acting on R1000)

N	R=1000mm			R=2000mm		
	Centrifugal force 1/R	Coriolis force 2N/d	Resultant force F_r=1/R+2N/d	Centrifugal force 1/R	Coriolis force 2N/d	Resultant force F_r=1/R+2N/d
-0.018				0.5	-0.72	-0.22
-0.012	1	-0.48	0.52	0.5	-0.48	0.02
0	1	0	1	0.5	0	0.5
0.012	1	0.48	1.48	0.5	0.48	0.98
0.018				0.5	0.72	1.32

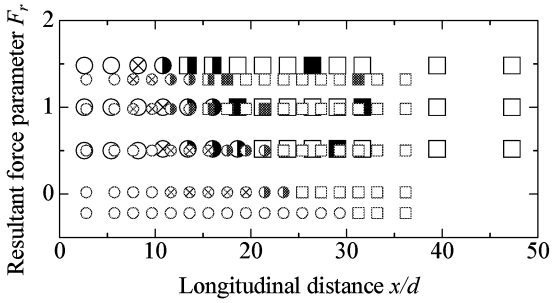

Fig. 12 Comparison between flow patterns of R1000mm and 2000mm (○:laminar state, ⊗:primary instability (Görtler vortices), ◑:secondary instability(varicose & sinuous mode), ◨:secondary instability(merge of vortices pairs), ■:merging of vortices pairs in turbulent state, ◧:turbulent state), large symbol; R1000mm, small symbol; R2000mm.

4. CONCLUSION

Detail measurement of the velocity inside the boundary layer along the concave wall is made and the occurrence and instability of the Görtler vortices as well as the transition to the turbulent state are examined. The results are summarized as follows.

(1) With the increase in the resultant force acting toward the concave wall, the pitch of the Görtler vortices decreases and the interaction among the vortices are enhanced, resulting in a sinuous mode of the secondary instability and the merge of the vortices. On the other hand, a varicose mode of secondary instability is observed when the resultant force is weakened. When the Coriolis force acts opposite to the concave wall and surpasses the centrifugal one, the occurrence of the Görtler vortices is suppressed.

(2) The occurrence of the secondary instability in the Görtler flow begins when the velocity nonuniformity due to the Görtler vortices exceeds a certain limit regardless of the system rotation.

(3) Occurrence of the Görtler vortices is roughly predicted by a parameter taking account for the effects of wall curvature and system rotation linearly. The prediction of the fluctuating flow nature, however, cannot be made by this parameter.

NOMENCULTURE

d : Width of the channel =50mm
G : Görtler number $= Re_\theta \sqrt{\theta / R}$
G' : Görtler number with rotating effect $= Re_\theta \sqrt{\theta(1/R + 2N/d)}$
N : Rotating rate (see eq.(1))
R : Wall curvature mm
Re : Reynolds number $= U_m d/\nu$
Re_θ : Reynolds number based on momentum thickness $= U_m \theta/\nu$
U : Time-averaged longitudinal velocity m/s
$\overline{U}$: Lateral mean time-averaged velocity m/s
U_m : Free stream velocity at most upstream section m/s
Ω : Rotational speed of channel rad/s

REFERENCES

Hämmerlin, G., 1955, "Über das Eigenwertprolem der dreidimensionalen Instabilität laminarer Grenzschichten an konkaven Wänden", J. Rat. Mech. Anal., Vol. 4, pp. 279-312.

Bradshaw, P., 1969, "The Analogy between Streamline Curvature and Buoyancy in Turbulent Shear Flow", Journal of Fluid Mechanics, Vol. 36, pp. 177-191.

Johnston, J. P., 1973, "The Suppression of Shear Layer Turbulence in Rotating Systems", Trans. ASME, Journal of Fluids Engineering, Vol. 95-1, pp. 229-239.

Koyama, H., Masuda, S., Ariga, I., and Watanabe, I., 1979, "Stabilizing and Destabilizing Effects of Coriolis Force on Two-dimensional Laminar and Turbulent Boundary Layers", Trans. ASME, Journal of Engng. Power, Vol.101, pp. 23-31.

Kikuyama, K., Nishibori, K., Hara, S., 1987, "Effects of System Rotation upon Turbulent Boundary Layer on a Concave Surface", Proc. 6th Sympo. on Turbulent Shear Flows, 1.4.1.

Swearingen, J.D. and Blackwelder, R.F., 1987, "The Growth and breakdown on the streamwise vortices in the presence of a wall", Journal of Fluid Mechanics, Vol. 182, pp. 255-290.

Matsson, O.J.E., and Alfredsson, P.H., 1992 "Experiments on instability in curved channel flow", Physics of Fluids A, Vol. 4, pp.1666-1676.

Matsson, O.J.E., and Alfredsson, P.H., 1994, "The effect of spanwise system rotation on Dean vortices", Journal of fluid Mechanics, Vol. 274, pp. 243-265.

Matsubara, M., and Alfredsson, P. H., 1998, "Secondary instability in rotating channel flow", Journal of Fluid Mechanics, Vol. 368, pp. 27-50.

Hasegawa, Y., Kikuyama, K., Nishikawa, M., and Ikeda, T., 2003, "Study of boundary layer flow in rotating curvature system (The occurrence and growth of streamwise vortices)", Proc. 3rd Int. Sympo. on Turbulent and Shear Flow Phenomena, pp. 461-466.